Satellite-based estimates of Antarctic surface meltwater fluxes

Luke D. Trusel,[1] Karen E. Frey,[1] Sarah B. Das,[2] Peter Kuipers Munneke,[3] and Michiel R. van den Broeke[3]

[1] This study generates novel satellite-derived estimates of Antarctic-wide annual (1999–2009) surface meltwater production using an empirical relationship between radar backscatter from the QuikSCAT (QSCAT) satellite and melt calculated from in situ energy balance observations. The resulting QSCAT-derived melt fluxes significantly agree with output from the regional climate model RACMO2.1 and with independent ground-based observations. The high-resolution (4.45 km) QSCAT-based melt fluxes uniquely detect interannually persistent and intense melt (>400 mm water equivalent (w.e.) year^{-1}) on interior Larsen C Ice Shelf that is not simulated by RACMO2.1. This supports a growing understanding of the importance of a föhn effect in this region and quantifies the resulting locally enhanced melting that is spatially consistent with recently observed Larsen C thinning. These new results highlight important cryosphere-climate interactions and processes that are presently not fully captured by the coarser-resolution (27 km) regional climate model. Citation: Trusel, L. D., K. E. Frey, S. B. Das, P. Kuipers Munneke, and M. R. van den Broeke (2013), Satellite-based estimates of Antarctic surface meltwater fluxes, *Geophys. Res. Lett.*, *40*, 6148–6153, doi:10.1002/2013GL058138.

1. Introduction

[2] Ice shelf thinning [*Holland et al.*, 2011], outlet glacier dynamics [*Pritchard and Vaughan*, 2007; *Miles et al.*, 2013], and abrupt ice shelf collapse [*Scambos et al.*, 2000; *van den Broeke*, 2005] have all been linked to surface melt that is prevalent across coastal Antarctica [*Trusel et al.*, 2012]. Ice core observations from the northeast Antarctic Peninsula (AP) in fact reveal a recent acceleration of melt intensity to levels unprecedented within the last 1000 years [*Abram et al.*, 2013]. However, regional climate modeling indicates that most Antarctic surface melt refreezes in place [*Kuipers Munneke et al.*, 2012a], making surface meltwater runoff a presently minor component of the overall surface mass balance [*Lenaerts et al.*, 2012]. Furthermore, while basal melting dominates observed surface height changes and

thinning across many Antarctic ice shelves [*Pritchard et al.*, 2012], surface melting is also integral to height reductions [*Ligtenberg et al.*, 2012] and thus interpretation of the relative importance of atmospheric and oceanic forcing in driving ice shelf change. As such, surface melt plays a complex and coupled role in the Antarctic cryosphere and deciphering the magnitude of its glaciological relevance and impacts mandates a robust understanding of its dynamics across space and time.

[3] Several methods currently exist for examining Antarctic surface melt, each with inherent limitations. Direct assessment of melt from ice core stratigraphy [e.g., *Das and Alley*, 2008; *Abram et al.*, 2013] and in situ surface energy balance (SEB) observations [e.g., *Kuipers Munneke et al.*, 2012b] provide robust melt records but are exceedingly rare and spatially constrained. Microwave satellites detect increases in brightness temperature [e.g., *Tedesco et al.*, 2007] or decreases in radar backscatter [e.g., *Barrand et al.*, 2013] during melt episodes. However, such observations may be biased by satellite overpass timing [*Picard and Fily*, 2006] or sensor and algorithm sensitivity [e.g., *Trusel et al.*, 2012] and typically only assess melt presence or absence. Coupled climate-snowpack models can simulate meltwater fluxes over space and time [e.g., *Kuipers Munneke et al.*, 2012a] yet rely upon the quality of reanalysis data used for model forcing, suffer from a lack of independent validation data sets, and generally provide results at spatial resolutions coarser than satellite observations.

[4] Here we develop the first quantitative, satellite-based estimates of Antarctic-wide surface meltwater production by utilizing radar backscatter time series from QuikSCAT (QSCAT) calibrated with SEB-derived melt flux observations. We explore these results in concert with regional climate model output from RACMO2.1 (hereafter RACMO) to assess both satellite and climate model results.

2. Methods

2.1. Satellite Melt Detection

[5] This study utilized 10 years (1999–2009) of radar backscatter (σ^0) time series from the SeaWinds scatterometer aboard QSCAT, consisting of daily pan-Antarctic, afternoon overpass data (1200–2000 h local time) at vertical polarization, with 4.45 km (~8–10 km effective) resolution [*Long*, 2010]. Satellite-derived melt detection followed the threshold-based methods of *Trusel et al.* [2012] (see supporting information for further details). For a variety of radar frequencies, an approximately inverse linear relationship has been documented between snowpack liquid water content (LWC) and backscatter up to a certain LWC threshold (~5% or greater) [e.g., *Stiles and Ulaby*, 1980]. Building upon this theory are findings of significant linear relationships between seasonally summed positive air temperatures

---
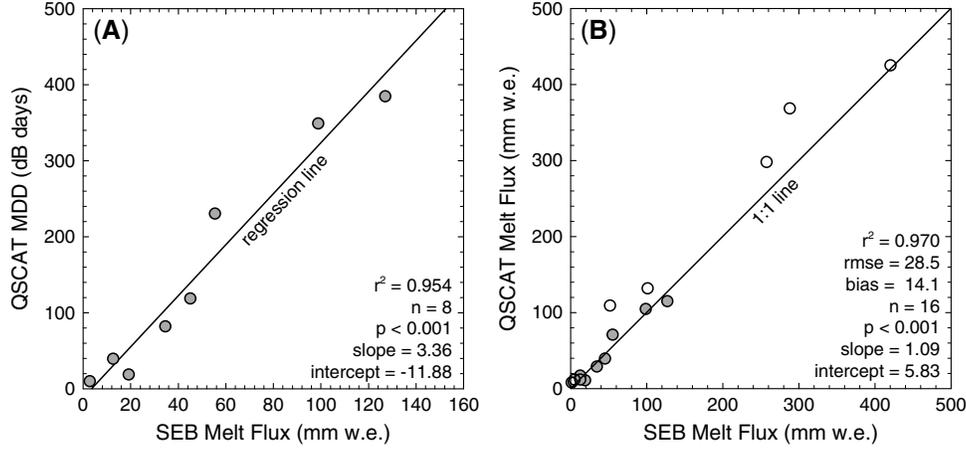
Figure 1. (a) Calibration between annual sums of QSCAT MDD- and SEB-based melt fluxes at Neumayer Station. (b) Evaluation of all available coincident QSCAT- and SEB-based melt fluxes across the five locations shown in Figure 2 (gray points from Neumayer calibration in Figure 1a).

(i.e., positive degree days) and radar backscatter during melt [*Wismann*, 2000; *Smith et al.*, 2003; *Trusel et al*, 2012]. Across Antarctica, *Trusel et al.* [2012] employed these relationships to estimate relative melt intensity, calculated as melting decibel days (MDD):

$$\text{MDD}_{\text{year } n+1} = \sum_{i=\text{day } 201, \text{ year } n}^{i=\text{day } 200, \text{ year } n+1} \text{MD}\left(\overline{\sigma_w^0} - \sigma_i^0\right) \qquad (1)$$

where σ_i^0 is the daily backscatter for a pixel, $\overline{\sigma_w^0}$ is the mean winter (July–September) backscatter of year n, and MD is a binary function expressing melt status. Here, MDD and daily backscatter reductions during melt were compared with meltwater fluxes obtained from SEB modeling to better assess backscatter-melt relationships and to empirically calibrate MDD with surface melt fluxes.

2.2. Melt Derived From Surface Energy Balance Modeling

[6] Quantifying surface melt is possible by evaluating the full SEB:

$$\begin{aligned} M &= \text{SW}_{\text{net}} + \text{LW}_{\text{net}} + \text{SHF} + \text{LHF} + \text{G}_s, \text{if } \text{T}_s = 0\,°\text{C} \\ M &= 0, \text{if } T_s < 0\,°\text{C} \end{aligned} \qquad (2)$$

where M is the energy available for melting, T_s is the snow surface temperature, SW_{net} and LW_{net} are the net shortwave and longwave radiative fluxes, SHF and LHF are the turbulent fluxes of sensible and latent heat, and G_s is the subsurface conductive heat flux evaluated at the surface. Here, we utilized SEB-derived melt fluxes calculated at five Antarctic sites: Neumayer Station [*van den Broeke et al.*, 2010; *König-Langlo*, 2013], Automated Weather Station (AWS) 14 and AWS 15 on Larsen C Ice Shelf [*Kuipers Munneke et al.*, 2012b], Larsen C AWS [*van den Broeke*, 2005], and Pine Island Glacier AWS A. At most locations (see supporting information for details), M was determined using radiative fluxes observed in situ, turbulent fluxes calculated via the bulk method, and G_s calculated by coupling the SEB to a snowpack model.

2.3. Melt Derived From Regional Climate Modeling

[7] Antarctic-wide surface melt was also determined using RACMO, which was two-way coupled to a multilayer snow model to calculate the SEB and simulate surface melt fluxes at a 27 km spatial resolution over 1979–2010 [*Kuipers Munneke et al.*, 2012a]. Here, daily output from RACMO was annually summed (mid July to mid July), matching the austral summer-centric QSCAT data set. Likewise, both QSCAT and RACMO were masked using an updated version of the MODIS-derived Antarctic coastline [*Haran et al.*, 2005]. When coupled to a snowpack model, SEB modeling and RACMO can simulate percolation, refreezing, and meltwater runoff. However, as scatterometers are most sensitive to near-surface melt [e.g., *Stiles and Ulaby*, 1980] and this study utilized solar afternoon satellite data, this analysis limited satellite comparisons to instantaneous melt fluxes at the ice sheet surface (i.e., *M* in equation (2)). We emphasize these melt fluxes do not specify the fate of melt (e.g., refreeze or runoff), rather simply the production and presence of melt at the ice sheet surface.

3. Results

3.1. QSCAT-SEB Comparisons

[8] At daily resolution, QSCAT melt backscatter variations (i.e., dB below the melt threshold) show a clear response to surface meltwater production as determined using the SEB method ($r^2 = 0.680$; Figure S1 in the supporting information). When annually summed, the relationship is far more robust: annual surface melt fluxes explain over 95% of the QSCAT MDD variability at Neumayer (Figure 1a). As such, we employed the Neumayer relationship to empirically model Antarctic-wide surface meltwater fluxes (in mm w.e. year^{-1}) from QSCAT MDD. We further evaluated the robustness of this relationship by comparing calibrated QSCAT melt fluxes and all available SEB-based observations over coincident annual and subannual time scales and find a similarly strong linear relationship ($r^2 = 0.970$; Figure 1b).

3.2. QSCAT-RACMO Comparisons

[9] Broad spatiotemporal agreement exists between QSCAT and RACMO, with coherent mean annual melt fluxes observed across much of Antarctica (Figure 2). The greatest surface melt
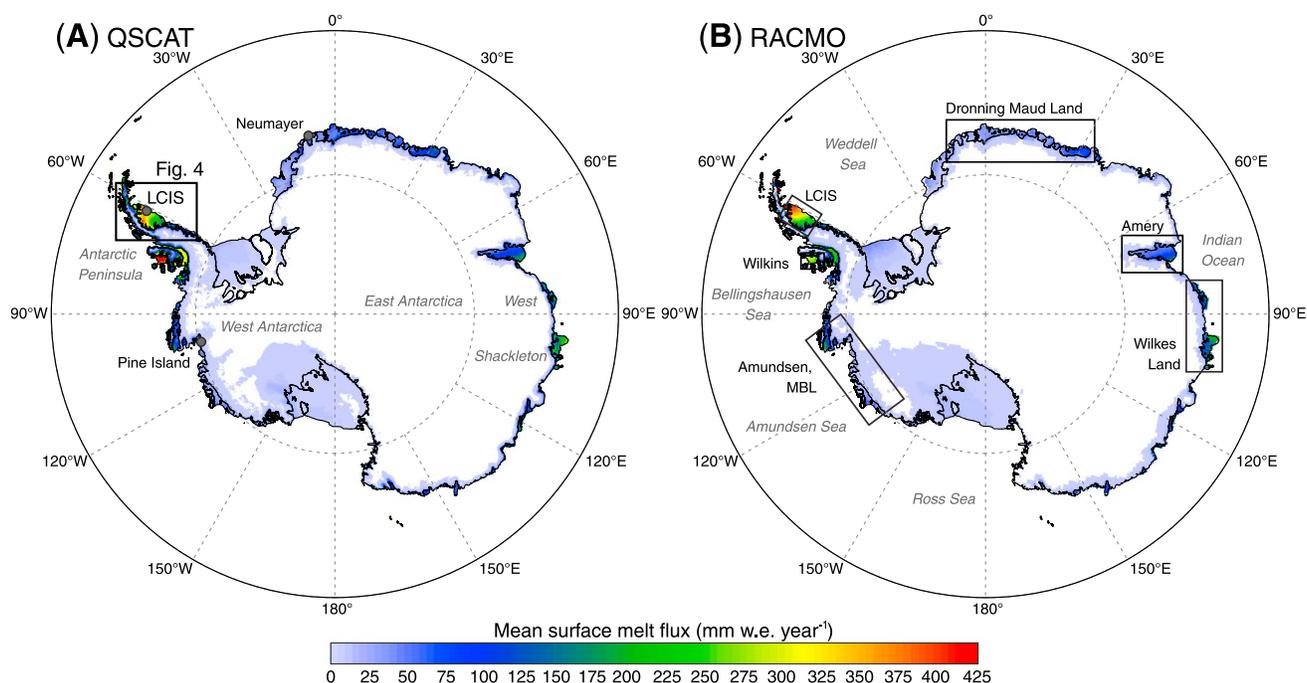
Figure 2. Plots of 10 year (1999–2009) mean surface melt fluxes from (a) QSCAT and (b) RACMO. Labeled gray dots in Figure 2a denote locations of SEB observations (LCIS includes Larsen C AWS, AWS 14, and AWS 15). Boxes in Figure 2b denote areas of profiles shown in Figure 3.

presently occurs on AP ice shelves. For example, both methods find melt on portions of Larsen C Ice Shelf (LCIS) in excess of 400 mm w.e. year^{-1}. On ice shelves of the western AP, QSCAT and RACMO observe similar spatial melt patterns, but QSCAT finds generally larger mean melt fluxes than RACMO (Figure 2). Beyond the AP, the most intense surface melt occurs on the outermost portions of Shackleton Ice Shelf in East Antarctica, where both methods indicate >200 mm w.e. year^{-1}. Across Dronning Maud Land, both methods observe the greatest melt on Roi Baudouin Ice Shelf (~30°E) and suggest an apparent orographic effect producing locally enhanced melt on inner Fimbul Ice Shelf (~0–4°E) (Figures 2 and S2). Similarly, QSCAT and RACMO observe peak melting on northeast Amery Ice Shelf (~150 mm w.e. year^{-1}). Generally low melt (several tens of mm w.e. year^{-1}) occurs on average across ice shelves bordering the Ross and Amundsen Seas and both methods capture anomalously extensive but low intensity West Antarctic Ice Sheet melt in 2004–2005, although RACMO simulates melt at higher elevation (>1600 m) than QSCAT (Figures 2 and S3).

[10] Interannual variations in the Antarctic-wide meltwater volume calculated by QSCAT and RACMO over 1999–2009 are significantly correlated, although QSCAT estimates ~30 Gt year^{-1} greater annual melt on average (Figure 3a). Spatially averaged melt fluxes over specific ice sheet and ice shelf areas are also highly correlated (Figures 3b–3g). Across LCIS, the magnitude and interannual variability of melt fluxes empirically estimated from QSCAT are largely reproduced by RACMO (Figure 3b). However, Wilkins Ice Shelf is representative of an overall western AP discrepancy between the methods. Here although moderately correlated, QSCAT estimates an average of ~100 mm w.e. year^{-1} greater melt than RACMO (Figure 3c).

[11] Figure 4 shows that despite producing similar melt fluxes for LCIS as a whole (e.g., Figure 3b), important spatial distinctions exist between QSCAT and RACMO. Specifically, QSCAT indicates a swath of enhanced melt across the Foyn and Bowman Coast Inlets of LCIS (~40% greater near Mill Inlet), whereas RACMO produces larger melt fluxes (~10% greater) across northernmost LCIS and the remnants of Larsen B in Scar Inlet (Figure 4). Profiles across central LCIS highlight differences in meltwater production and spatial resolution (Figure 4c). In particular, QSCAT observes peak melting on the leeward side of the AP mountains that gradually decreases toward the Weddell Sea, whereas RACMO shows monotonically increasing melt toward the outer ice shelf, consistent with trends in melt duration [*Barrand et al.*, 2013].

4. Discussion and Conclusions

[12] Empirical estimation of Antarctic surface meltwater production from QSCAT is supported by agreement with two fully independent data sets generated from ground SEB observations and regional climate modeling. SEB modeling, although sparse, enables calibration between MDD and melt fluxes and supports the linearity of this Antarctic backscatter-melt relationship across a broad range of melt conditions and time scales (Figures 1 and S1). This confirmation is important given potential complexities including the relative insensitivity of radar backscatter to melt variations at high LWC [*Stiles and Ulaby*, 1980], and the backscatter reliance upon specific snowpack conditions [e.g., *Nghiem et al.*, 2001]. We note that under persistently high snowpack LWC, continuous daily exhaustion of the backscatter dynamic range would likely result in underestimation of the annual melt flux using this method. However, significant
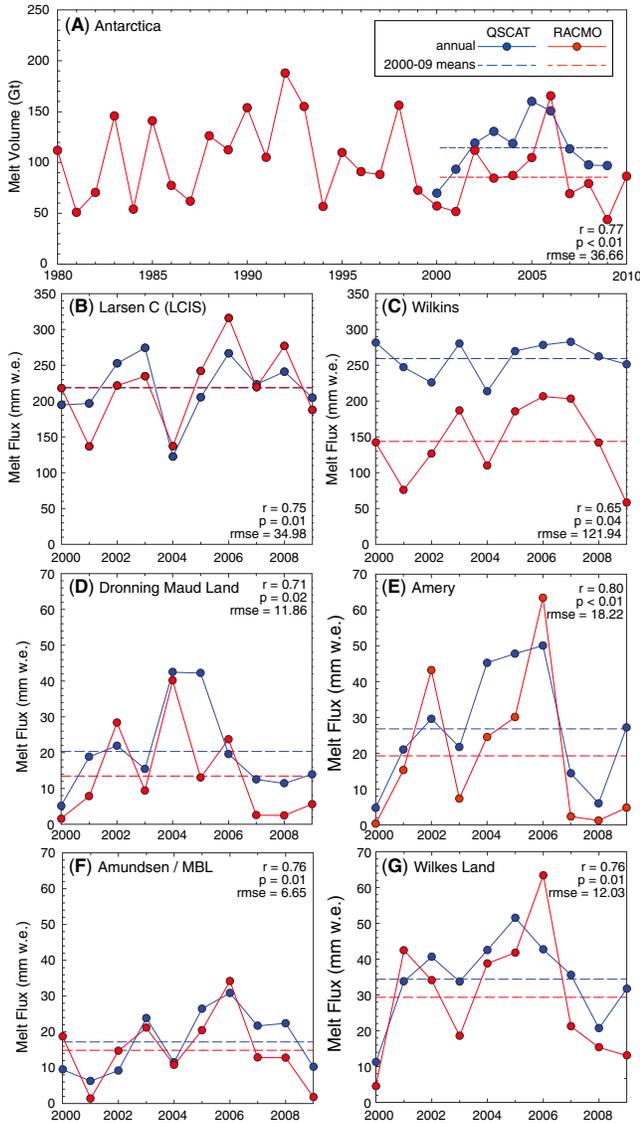
Figure 3. (a) Total Antarctic-wide surface melt volume. (b–g) Melt fluxes (left axes) from QSCAT (blue) and RACMO (red) across ice sheet and shelf locations (see Figure 2). Dashed lines show melt means over 1999–2009. Years refer to the second austral summer year (i.e., summer 1999–2000 is labeled 2000).

agreement between QSCAT and SEB melt results (Figure 1b; across nearly the full spectrum of melting presently experienced in Antarctica) indicates such saturation is not consistently met, and thus, a linear function well approximates the annual backscatter-melt relationship across Antarctica. Consistency between QSCAT and RACMO further validates this finding (Figures 2 and 3). Likewise, these agreements provide a unique resource for assessing the performance of RACMO across broad spatial scales over Antarctica and indicate largely reliable results from both RACMO and QSCAT methods over 1999–2009. Nonetheless, future in situ SEB observations across underrepresented regions of Antarctica subject to surface melting would provide even further confidence and utility in assessing both satellite and climate model products.

[13] Although melt fluxes from QSCAT and RACMO largely agree, several discrepancies exist that warrant further discussion. First, the greater average continent-wide melt volume of QSCAT (Figure 3a) reflects measurement of a larger coastal and ice shelf area by QSCAT (~350,000 km^2 greater) owing to its finer spatial resolution (4.45 km; e.g., Figure 4). Second, comparisons at Neumayer Station (Figure S1) and beyond (Figure S3) indicate that RACMO underpredicts melt fluxes during 2004–2005 across East Antarctica, contributing to divergences with QSCAT. At Neumayer, this melt underestimation appears to result from snowfall events occurring on and just before the day of initial melt onset (as observed by QSCAT and the in situ SEB), which raised albedo (i.e., decreased SW_{net}), thus inhibiting melt initiation and the consequential melt-albedo feedback necessary to accurately represent seasonal surface melt (Figure S4). Finally, on the western AP, QSCAT observed higher mean melt fluxes than RACMO (e.g., Figure 2). In a similar study, *Barrand et al.* [2013] concluded that RACMO grid coarseness, as well as the QSCAT response to (and lack of RACMO treatment of) ponding, likely resulted in RACMO underprediction of melt duration relative to QSCAT. We also find resolution-dependent melt flux underestimation in RACMO (e.g., the 25–30 km wide northern George VI Ice Shelf) owing to its coarse topography and the strong inverse relationship between melt and elevation. However, although meltwater ponding likely leads to some further divergence between RACMO and QSCAT on the western AP, ponds are not ubiquitous across all ice shelves (notably Wilkins), and our pan-Antarctic analysis does not observe similar discrepancies where surface melt features exist elsewhere (e.g., Scar Inlet and Amery Ice Shelf). As such, systematically lower western AP melt fluxes in RACMO (yet consistency with QSCAT on other ice shelves of similar size, topographic complexity, and melt feature coverage) suggest factors other than ponding and spatial resolution may be responsible. Potential explanations include coarse model simulation of coastal climate on the western AP and (particularly for Wilkins and adjacent ice shelves) an insufficient simulation of a föhn effect in the lee of Alexander Island during particular prevailing wind directions.

[14] Across the northeastern AP and Larsen Ice Shelf, adiabatically warmed and dried föhn winds have been linked to higher air temperatures [*Marshall et al.*, 2006], decreased surface mass balance [*van Lipzig et al.*, 2008], and heightened surface melt fluxes [*Kuipers Munneke et al.*, 2012b] and duration [*Trusel et al.*, 2012; *Barrand et al.*, 2013]. Our QSCAT results uniquely reveal amplified melt fluxes across a broad swath of interior LCIS (Figure 4) that are a persistent feature of the satellite record (Figure S5) and accordant with the influence of a pervasive föhn impact on the SEB. RACMO at 27 km resolution, conversely, does not show similar melt patterns (Figure 4b) likely owing to insufficient simulation of föhn winds as was shown to result from topographic smoothing in coarser-grid RACMO runs [*van Lipzig et al.*, 2008] and identified in comparisons between QSCAT and RACMO melt duration [*Barrand et al.*, 2013]. As much of inner and northern LCIS has low firn air content [*Holland et al.*, 2011], enhanced melting across this area can lead to an expansion of existing surface ponding (Figure S6), albedo reduction, and associated positive feedback mechanisms promoting further melt, ponding, and ice shelf thinning. Indeed, the melt pattern observed by QSCAT largely mirrors patterns of recent
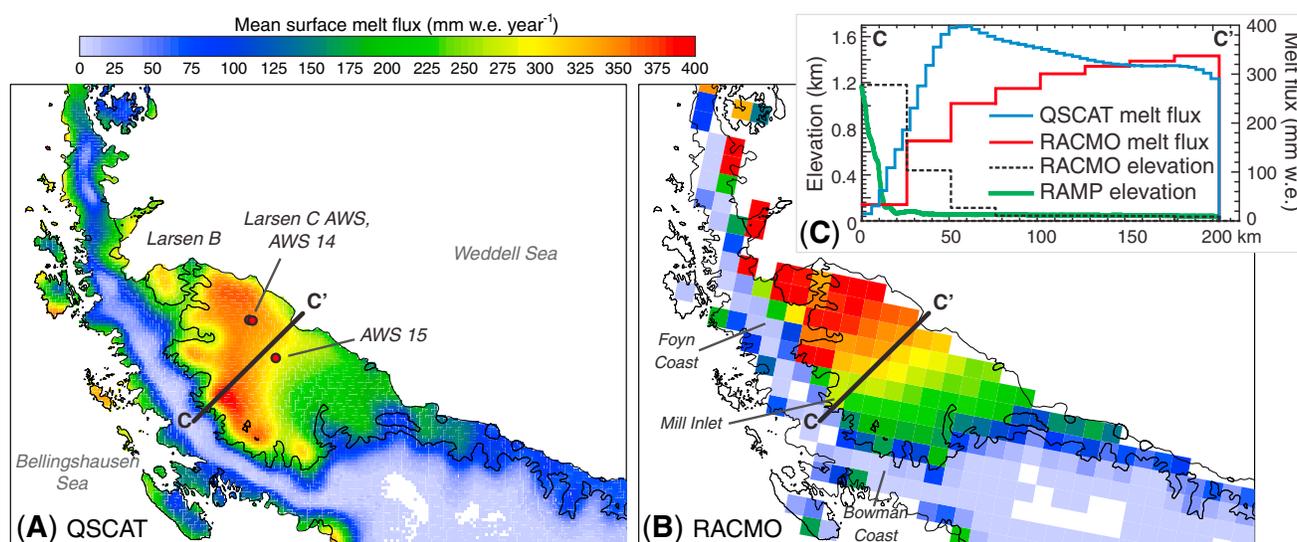
Figure 4. Mean melt fluxes over 1999–2009 across the northern Antarctic Peninsula from (a) QSCAT and (b) RACMO. (c) Profiles along C–C' of mean melt fluxes from QSCAT (blue) and RACMO (red), as well as elevation from RACMO (dashed black) and RAMP (green) [*Liu et al.*, 2001]. Location of this region is indicated in Figure 2.

LCIS thinning [*Pritchard et al.*, 2012], affirming surface melt as an important component of LCIS surface lowering. Accordingly, monitoring of melt, near-surface atmospheric and firn conditions (including föhn impacts), and ice shelf thinning across LCIS are all imperative to assessing its potential vulnerability to melt-induced destabilization.

[15] This paper presents the first satellite-based surface melt flux estimates for Antarctica. We find an overall agreement with ground-based melt fluxes as well as those from the regional climate model RACMO. Areas of disagreement between satellite and climate model results point to the necessity of observing and modeling Antarctic melt processes at sufficiently high spatial resolution. Barring such observations, important cryosphere-climate interactions and associated glaciological impacts of surface melt (e.g., föhn winds driving Larsen Ice Shelf melt, ponding, and thinning) may not be fully realized.

References

Abram, N. J., R. Mulvaney, E. W. Wolff, J. Triest, S. Kipfstuhl, L. D. Trusel, F. Vimeux, L. Fleet, and C. Arrowsmith (2013), Acceleration of snow melt in an Antarctic Peninsula ice core during the twentieth century, *Nat. Geosci.*, *6*(5), 404–411, doi:10.1038/ngeo1787.

Barrand, N. E., D. G. Vaughan, N. Steiner, M. Tedesco, P. Kuipers Munneke, M. R. van den Broeke, and J. S. Hosking (2013), Trends in Antarctic Peninsula surface melting conditions from observations and regional climate modeling, *J Geophys. Res. Earth Surface*, *118*, 315–330, doi:10.1029/2012JF002559.

Das, S. B., and R. B. Alley (2008), Rise in frequency of surface melting at Siple Dome through the Holocene: Evidence for increasing marine influence on the climate of West Antarctica, *J. Geophys. Res.*, *113*, D02112, doi:10.1029/2007JD008790.

Haran, T., J. Bohlander, T. Scambos, T. Painter, and M. Fahnestock (2005), *MODIS Mosaic of Antarctica (MOA) Image Map*, National Snow and Ice Data Center, Boulder, Colorado USA.

Holland, P. R., H. F. J. Corr, H. D. Pritchard, D. G. Vaughan, R. J. Arthern, A. Jenkins, and M. Tedesco (2011), The air content of Larsen Ice Shelf, *Geophys. Res. Lett.*, *38*, L10503, doi:10.1029/2011GL047245.

König-Langlo, G. (2013), Basic measurements of radiation from Neumayer Station in the year 1999–2007, Alfred Wegener Institute, Helmholtz Center for Polar and Marine Research, Bremerhaven, doi:10.1594/PANGAEA.819774.

Kuipers Munneke, P., G. Picard, M. R. van den Broeke, J. T. M. Lenaerts, and E. van Meijgaard (2012a), Insignificant change in Antarctic snowmelt volume since 1979, *Geophys. Res. Lett.*, *39*, L01501, doi:10.1029/2011GL050207.

Kuipers Munneke, P., M. R. van den Broeke, J. C. King, T. Gray, and C. H. Reijmer (2012b), Near-surface climate and surface energy budget of Larsen C ice shelf, Antarctic Peninsula, *The Cryosphere*, *6*(2), 353–363, doi:10.5194/tc-6-353-2012.

Lenaerts, J. T. M., M. R. van den Broeke, W. J. van de Berg, E. van Meijgaard, and P. K. K. Munneke (2012), A new, high-resolution surface mass balance map of Antarctica (1979–2010) based on regional atmospheric climate modeling, *Geophys. Res. Lett.*, L04501, doi:10.1029/2011GL050713.

Ligtenberg, S. R. M., M. Horwath, M. R. van den Broeke, and B. Legrésy (2012), Quantifying the seasonal "breathing" of the Antarctic ice sheet, *Geophys. Res. Lett.*, *39*, L23501, doi:10.1029/2012GL053628.

Liu, H., K. Jezek, B. Li, and Z. Zhao (2001), Radarsat Antarctic Mapping Project digital elevation model version 2. Boulder, Colorado USA: National Snow and Ice Data Center. Digital media.

Long, D. G. (2010), Standard BYU QuikSCAT and Seawinds land/ice image products, Brigham Young University, Microwave Earth Remote Sensing Laboratory.

Marshall, G. J., A. Orr, N. P. M. van Lipzig, and J. C. King (2006), The impact of a changing Southern Hemisphere annular mode on Antarctic Peninsula summer temperatures, *J. Clim.*, *19*(20), 5388, doi:10.1175/JCLI3844.1.

Miles, B. W. J., C. R. Stokes, A. Vieli, and N. J. Cox (2013), Rapid, climate-driven changes in outlet glaciers on the Pacific coast of East Antarctica, *Nature*, *500*(7464), 563–566, doi:10.1038/nature12382.

Nghiem, S. V., K. Steffen, R. Kwok, and W. Y. Tsai (2001), Detection of snowmelt regions on the Greenland ice sheet using diurnal backscatter change, *J. Glaciol.*, *47*, 539–547, doi:10.3189/172756501781831738.

Picard, G., and M. Fily (2006), Surface melting observations in Antarctica by microwave radiometers: Correcting 26-year time series from changes in acquisition hours, *Remote Sens. Environ.*, *104*(3), 325–336, doi:10.1016/j.rse.2006.05.010.

Pritchard, H. D., and D. G. Vaughan (2007), Widespread acceleration of tidewater glaciers on the Antarctic Peninsula, *J. Geophys. Res.*, *112*, F03S29, doi:10.1029/2006JF000597.

Pritchard, H. D., S. R. M. Ligtenberg, H. A. Fricker, D. G. Vaughan, M. R. van den Broeke, and L. Padman (2012), Antarctic ice-sheet loss driven by basal melting of ice shelves, *Nature*, *484*(7395), 502–505, doi:10.1038/nature10968.

Scambos, T. A., C. Hulbe, M. Fahnestock, and J. Bohlander (2000), The link between climate warming and break-up of ice shelves in the Antarctic Peninsula, *J. Glaciol.*, *46*, 516–530, doi:10.3189/172756500781833043.

Smith, L. C., Y. Sheng, R. R. Forster, K. Steffen, K. E. Frey, and D. E. Alsdorf (2003), Melting of small Arctic ice caps observed from ERS scatterometer time series, *Geophys. Res. Lett.*, *30*(20), 2034, doi:10.1029/2003GL017641.

Stiles, W. H., and F. T. Ulaby (1980), The active and passive microwave response to snow parameters 1. Wetness, *J. Geophys. Res.*, *85*(C2), 1037–1044.

Tedesco, M., W. Abdalati, and H. J. Zwally (2007), Persistent surface snowmelt over Antarctica (1987–2006) from 19.35 GHz brightness temperatures, *Geophys. Res. Lett.*, *34*, L18504, doi:10.1029/2007GL031199.

Trusel, L. D., K. E. Frey, and S. B. Das (2012), Antarctic surface melting dynamics: Enhanced perspectives from radar scatterometer data, *J. Geophys. Res.*, *117*, F02023, doi:10.1029/2011JF002126.

van den Broeke, M. (2005), Strong surface melting preceded collapse of Antarctic Peninsula ice shelf, *Geophys. Res. Lett.*, *32*, L12815, doi:10.1029/2005GL023247.

van den Broeke, M., G. König-Langlo, G. Picard, P. Kuipers Munneke, and J. Lenaerts (2010), Surface energy balance, melt and sublimation at Neumayer Station, East Antarctica, *Antarct. Sci.*, *22*(1), 87–96, doi:10.1017/S0954102009990538.

van Lipzig, N. P. M., G. J. Marshall, A. Orr, and J. C. King (2008), The Relationship between the Southern Hemisphere annular mode and Antarctic Peninsula summer temperatures: Analysis of a high-resolution model climatology, *J. Clim.*, *21*(8), 1649–1668, doi:10.1175/2007JCLI1695.1.

Wismann, V. (2000), Monitoring of seasonal snowmelt on Greenland with ERS scatterometer data, *IEEE Trans. Geosci. Remote Sens.*, *38*(4), 1821–1826, doi:10.1109/36.851766.